JOURNAL OF MATERIALS SCIENCE 26 (1991) 1485–1496

Comparative study of spinodal decomposition in symmetric and asymmetric Cu–Ni–Cr alloys

P. PRASAD RAO
Department of Metallurgical Engineering, Karnataka Regional Engineering College, Surathkal, Karnataka, 574 157, India

B. K. AGRAWAL, A. M. RAO
Department of Metallurgical Engineering, Indian Institute of Technology, Bombay, 400 076, India

Spinodal decomposition in three alloys of nominal compositions 71Cu–27Ni–2Cr, 45Cu–45Ni–10Cr and 33Cu–52Ni–15Cr were studied by X-ray diffraction technique and transmission electron microscopy. It was found that the first and third alloys are asymmetric in nature while the second is symmetric. The symmetric alloy was found to decompose faster than the asymmetric ones. The asymmetry of the side bands was found to be related to the proportion of phases in the alloy. Electron microscopic studies revealed that during coarsening the major phase increases its connectivity by isolating the minor phase.

1. Introduction

The existence of a miscibility gap in the Cu–Ni–Cr system was first reported by Meijering and coworkers [1]. The occurrence of the spinodal decomposition in these alloys was first reported by Manenc [2]. Since then studies have been carried out on the transformation characteristics and strengthening mechanism in several alloys spanning the miscibility gap [3–8]. All these have unambiguously proved that spinodal decomposition does occur in the alloys lying within the miscibility gap.

The study of the decomposition in a series of alloys spanning the miscibility gap is useful in comparing the behaviour of symmetric and asymmetric alloys. Symmetric alloys are those which have equal volume fractions of the two low temperature phases while the asymmetric alloys have unequal volume fractions of these two low temperature phases.

Since the transformation in spinodal decomposition is essentially a diffusional process, the rate of decomposition should be proportional to the interdiffusion flux. This flux being higher for the symmetric alloy, it should decompose faster than the asymmetric alloys. Even though Bower *et al.* [5] have studied the spinodal decomposition in a series of Cu–Ni–Cr alloys, they have primarily done microstructural and not kinetic studies. Saunderson *et al.* [7] have also studied a series of Cu–Ni–Cr alloys but have investigated only the late stage coarsening kinetics. Both these studies are based on electron microscopic investigations. There is no systematic X-ray diffraction study of the decomposition process in these alloys. Hence it was decided to take up a study of the transformation characteristics of symmetric and asymmetric Cu–Ni–Cr alloys through the X-ray diffraction technique.

2. Experimental work

Alloys of nominal compositions indicated in Fig. 1 were prepared in the laboratory by melting electrolytic copper rods (99.96%), electrolytic grade nickel sheets (99.8%) and commercial purity 80–20 nichrome rods in an induction furnace. Chill cast ingots were homogenized at 1373 K for 36 h. Strips of 10 × 25 × 100 mm^3 cut from these ingots were initially hot rolled to 2 mm thickness at 1273 K and subsequently cold rolled to 1 mm thickness for X-ray diffraction work or to 300 μm thickness for transmission electron microscopy. The final chemical analysis as carried out on the cold-rolled materials using atomic absorption spectrophotometry is given in Table I.

All heat treatments were carried out in a Kanthal wound vertical tube furnace under an atmosphere of flowing argon. The samples were initially solution treated at 1273 K for 30 min and quenched into a bath of iced brine maintained at 258 K. These samples were subsequently aged for different lengths of time at 773, 823, 873, 923, 973 and 1073 K.

Hardness was measured on a Vickers hardness tester using a load of 10 kg.

X-ray diffraction studies were carried out on electropolished samples of dimension 1 × 30 × 50 mm^3 on a Philips diffractometer using a copper target and nickel filter. The (2 0 0) diffraction profile was scanned at a speed of 0.25° 2θ min^{-1}. A scanning range of 3° on either side of the Bragg peak was found to be adequate to record both the side bands associated with the profile.

Foils for electron microscopy were prepared by the window technique using an electrolyte of 75 vol % perchloric acid in glacial acetic acid at room temperature and 60 V for alloys B and C. The foils were

0022–2461/91 $03.00 + .12

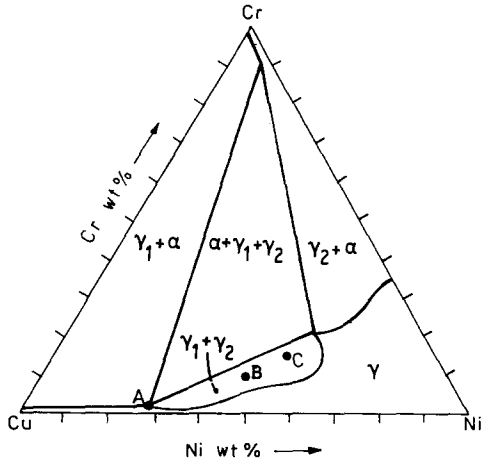

Figure 1 Isothermal section of Cu–Ni–Cr system at 1203 K showing the nominal compositions of the three alloys (after Meijering *et al.* [1]).

TABLE I Compositions of the alloys (wt %)

	Alloy	Ni	Cr	Cu
A	Nominal	27.00	2.00	71.00
	Actual	26.73	1.84	Bal.
B	Nominal	45.00	10.00	45.00
	Actual	44.78	9.61	Bal.
C	Nominal	52.00	15.00	33.00
	Actual	51.91	14.81	Bal.

studied in a Philips transmission electron microscope at 80 or 100 kV.

3. Results and discussion

3.1. Hardness measurements

Variation in hardness with ageing time at four ageing temperatures of 773, 873, 973 and 1073 K for the three alloys A, B and C are shown in Figs 2, 3 and 4, respectively. Curves in Fig. 2 are taken from Prasad Rao *et al.* [8] for the sake of comparison. It is seen from these figures that at all four temperatures, alloy B takes longer to reach the peak hardness than alloys A or C. At low ageing temperature of 773 K none of the alloys have reached the peak hardness and therefore the difference is not very significant. The difference is very pronounced at higher ageing temperatures of 973 or 1073 K.

It is further seen that transformation is fairly rapid at these higher temperatures. An early peak and a rapid fall in hardness beyond the peak indicate rapid coarsening, early onset of incoherency and formation of equilibrium phases.

X-ray diffraction studies were carried out on samples aged for different lengths of time at these temperatures with a view to studying the equilibrium phases.

X-ray diffraction studies were also carried out on samples aged at 773, 823, 873 and 923 K with a view to studying the kinetics of spinodal decomposition. At these low temperatures, decomposition proceeded

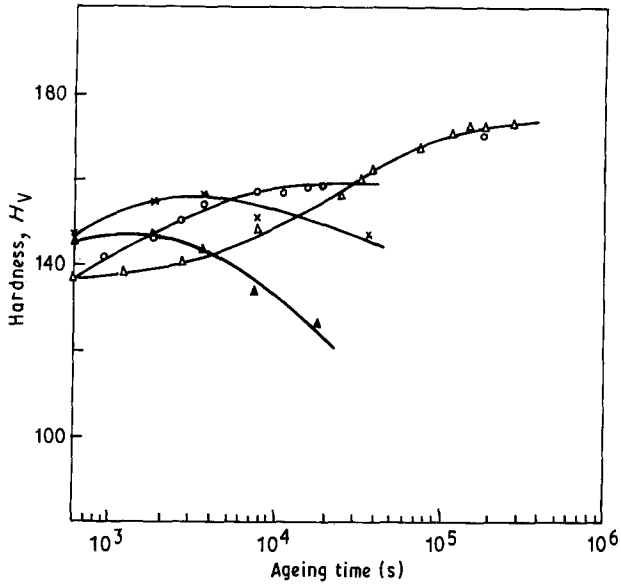

Figure 2 Variation in hardness with ageing time for alloy A at various ageing temperatures [8]. (▲ 1073 K, × 973 K, ○ 873 K, △ 773 K).

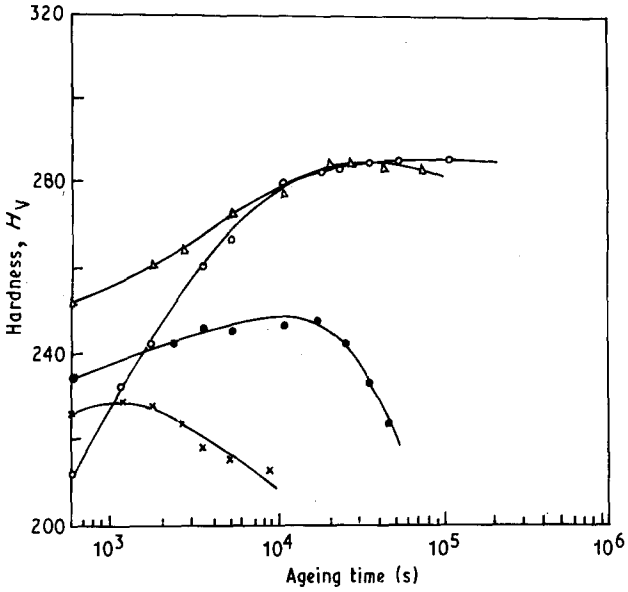

Figure 3 Variation in hardness with ageing time for alloy B at various ageing temperatures. (× 1073 K, ● 973 K, △ 873 K, ○ 773 K).

rather slowly as indicated by the variation in hardness. This afforded a study of the early stages of spinodal decomposition.

3.2. X-ray diffraction studies

3.2.1. Equilibrium phases

The X-ray diffraction profiles for the three alloys after ageing for different durations of time at 973 K are shown in Figs 5 to 7. For short ageing periods, well defined side bands were visible on either side of the Bragg peak. With continued ageing these approached the Bragg peak and merged with it making it rather broad at the base. On further ageing a second peak started appearing on the high angle side for alloy A and on the low angle side for alloy C. These are indicated by arrows in Figs 5 and 7, respectively. In

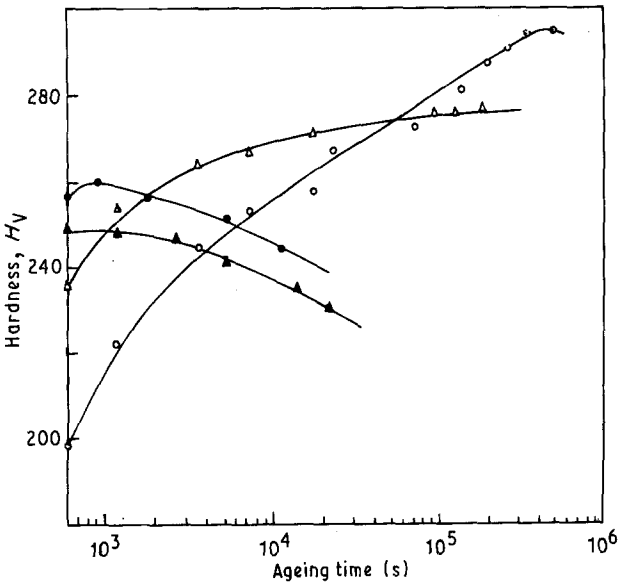

Figure 4 Variation in hardness with ageing time for alloy C at various ageing temperatures. (▲ 1073 K, ● 973 K, △ 873 K, ○ 773 K).

alloy B, after prolonged ageing, the entire Bragg peak became very broad and then split into two peaks on further ageing as shown in Fig. 6.

The appearance of the second peak was seen clearly on ageing at 1073 K. This is shown in Figs 8 to 10 for the three alloys after subjecting the profiles to Rachinger analysis [9]. From a consideration of the peak intensities it was concluded that the high lattice parameter constituent is the major phase in alloy A while the low lattice parameter constituent is the major phase in alloy C. In alloy B the two phases are approximately in equal proportion. Since the two phases in equilibrium in this system are copper-rich γ_1 and nickel-rich γ_2 phases, from a knowledge of the lattice parameters of the Cu–Ni system [10], the high lattice parameter phase can be identified as γ_1 and the low lattice parameter phase as γ_2. The lattice parameters and volume fractions of the two phases in equilibrium after long periods of ageing at 1073 K are given in Table II. These are estimated from the X-ray diffraction profiles of Figs 8 to 10.

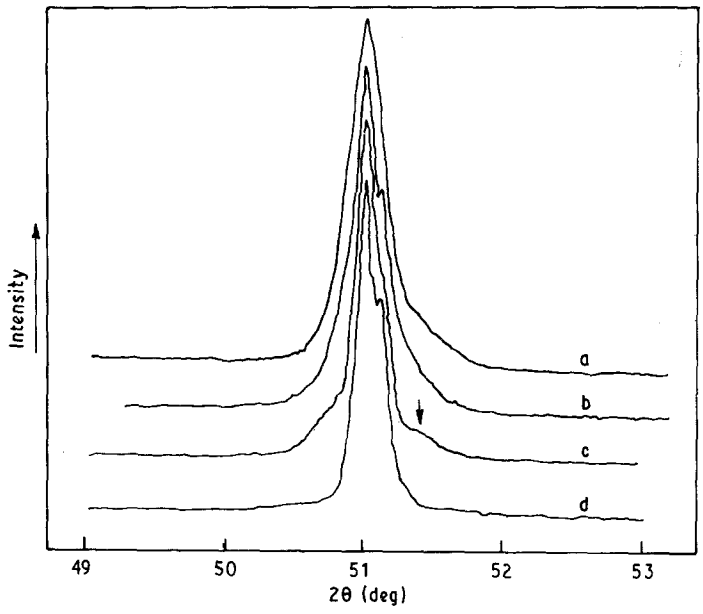

Figure 5 The X-ray diffraction profiles of alloy A on ageing at 973 K for different durations. (a 144 k sec, b 18 k sec, c 1200 sec, d 150 sec).

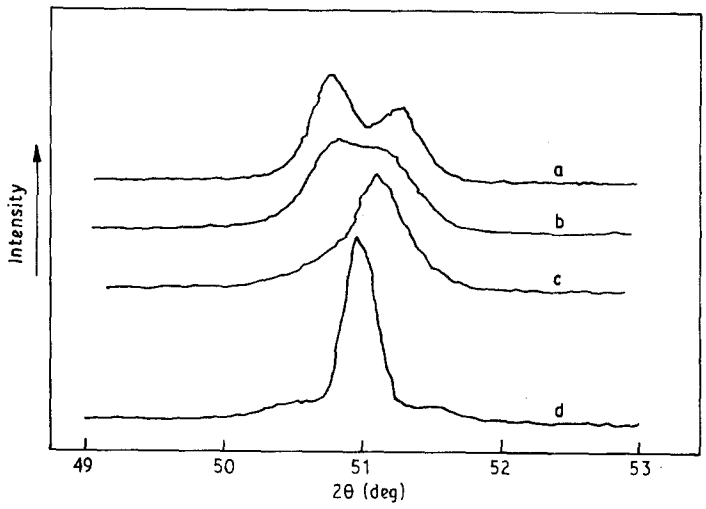

Figure 6 The X-ray diffraction profiles of alloy B on ageing at 973 K for various durations. (a 144 k sec, b 108 k sec, c 72 k sec, d 36 k sec).

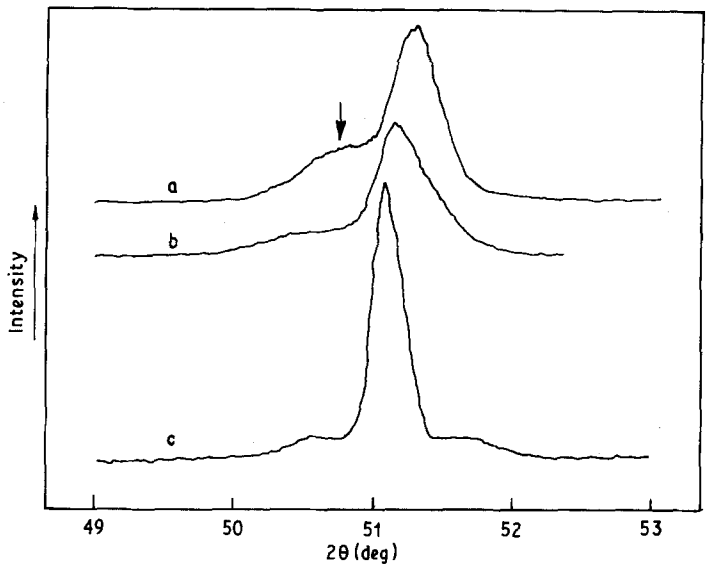

Figure 7 The X-ray diffraction profiles of alloy C on ageing at 973 K for various durations. (a 108 k sec, b 36 k sec, c 600 k sec).

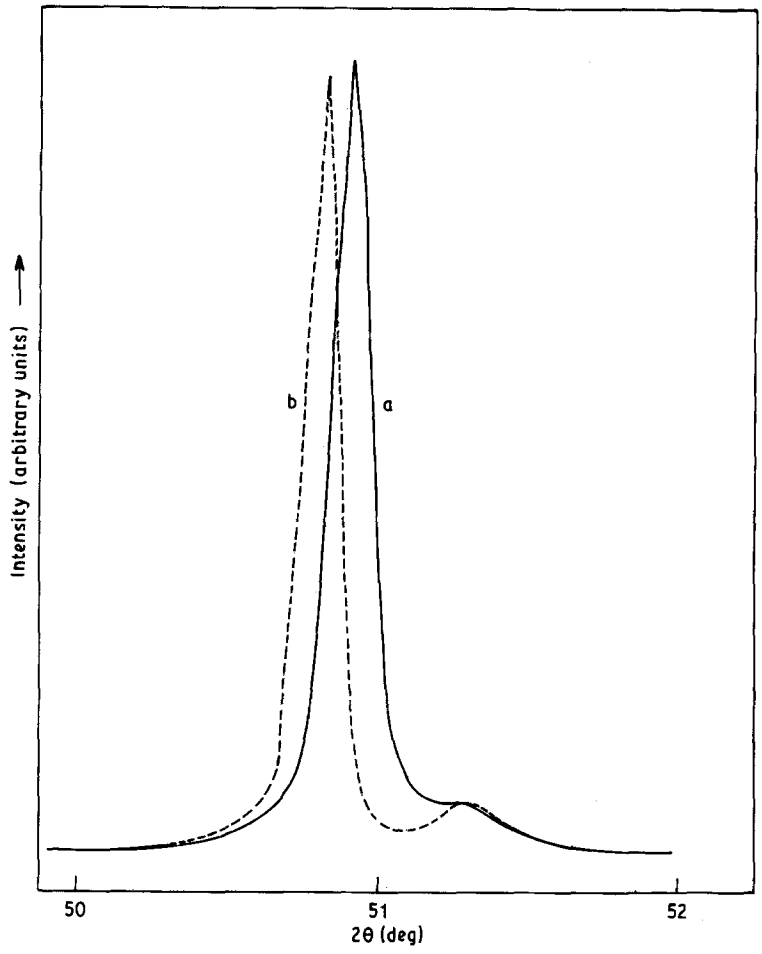

Figure 8 X-ray diffraction profiles of alloy A on ageing at 1073 K for (a) 36 k sec and (b) 396 k sec.

Of the three alloys under consideration, A and C are thus of asymmetric composition while B is of nearly symmetric composition.

3.2.2. Early stage decomposition

One of the most important features of the X-ray diffraction profiles of spinodally decomposing alloys is the occurrence of side bands on either side of the Bragg peak. Daniel and Lipson [11] showed that either a modulation in scattering factor or a modulation in lattice parameter due to composition modulation in an alloy should give rise to side bands in its X-ray diffraction profiles. They derived the following simple relationship between the angular separation, $\Delta\theta$, of the side band from the Bragg peak and wavelength, λ, for such a modulation

$$\lambda = \frac{ha_0 \tan \theta_B}{(\Delta\theta)(h^2 + k^2 + l^2)} \quad (1)$$

where hkl are the Miller indices of the Bragg peak, θ_B is the Bragg angle and a_0 is the average lattice parameter.

Ever since Hillert [12] showed that inside the spinodal periodic variations of composition occur which

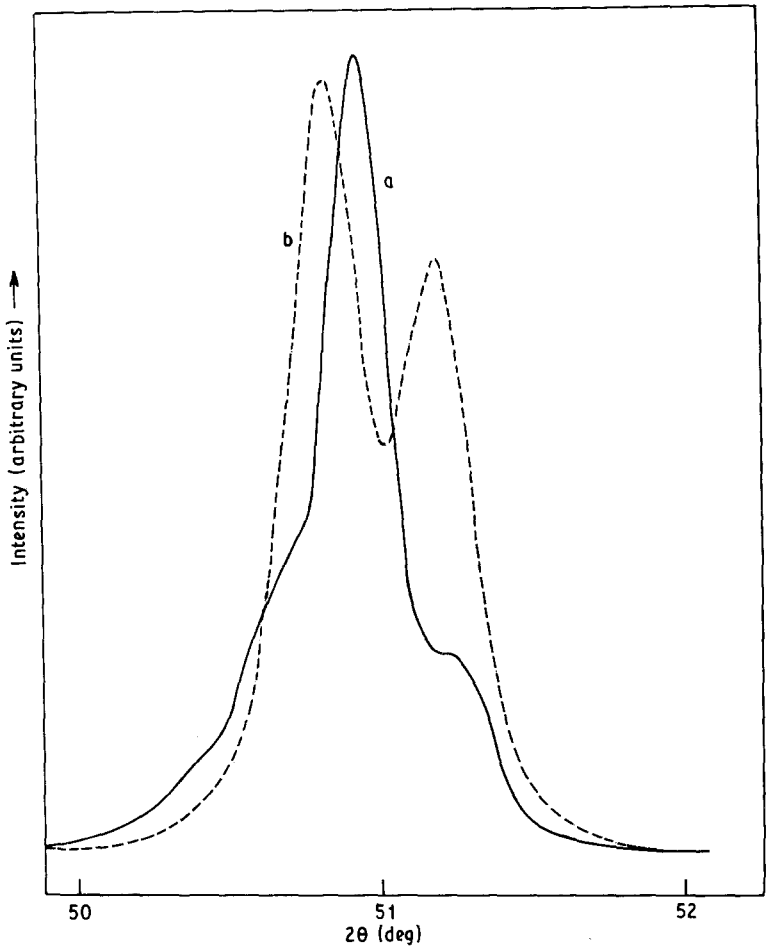

Figure 9 X-ray diffraction profiles of alloy B on ageing at 1073 K for (a) 3.6 k sec and (b) 36 k sec.

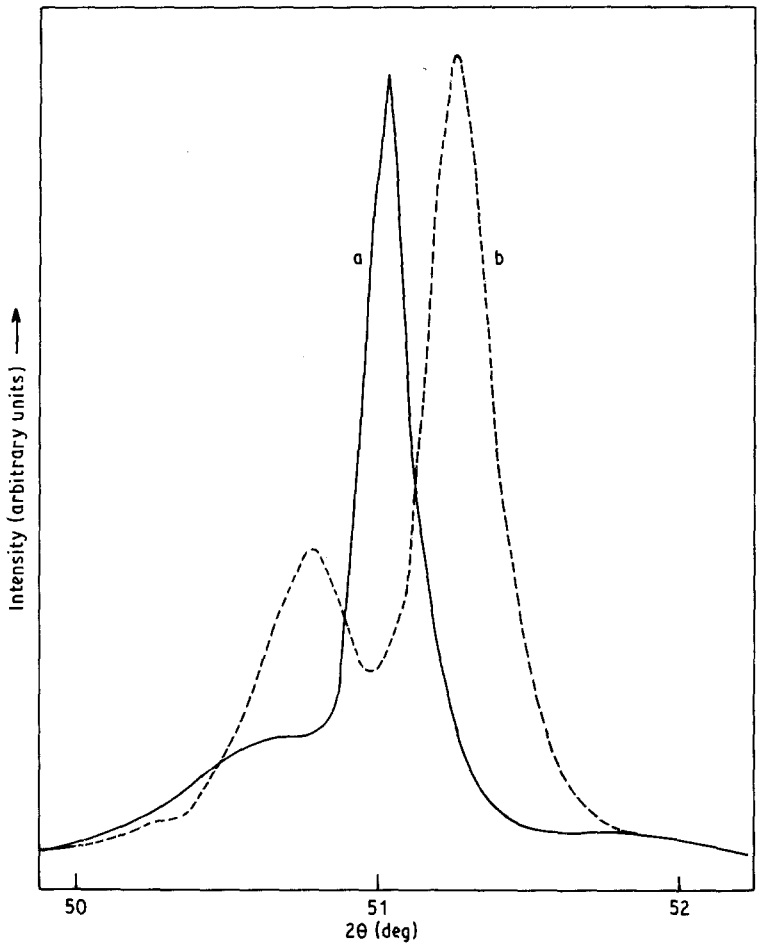

Figure 10 X-ray diffraction profiles of alloy C on ageing at 1073 K for (a) 3.6 k sec and (b) 36 k sec.

TABLE II Volume fractions and lattice parameters of equilibrium phases in alloys A, B and C after ageing at 1073 K.

Alloy	γ_1		γ_2	
	Lattice parameter (nm)	Volume fraction	Lattice parameter (nm)	Volume fraction
A	0.3589	0.91	0.3564	0.09
B	0.3590	0.55	0.3565	0.45
C	0.3592	0.31	0.3560	0.69

grow in amplitude and wavelength as the equilibrium phase separation was approached, it has been recognized that spinodally decomposing alloys should show side bands in their X-ray diffraction profiles. The Daniel–Lipson formula given above is the commonly accepted procedure for determining the wavelength. For the present investigation also this procedure has been followed.

Side bands were clearly observed on either side of the Bragg peaks of aged alloys. A set of profiles obtained for alloy B after ageing for different lengths of time at 873 K are shown in Fig. 11. These profiles are a combination of those due to α_1 and α_2 components of the X-radiation. These were, therefore, subjected to Rachinger analysis [9] to separate the two components. Such a set of profiles resulting from Rachinger analysis for alloy C are shown in Fig. 12. All the data from X-ray diffraction profiles reported in this work are those obtained from the α_1 component of the X-radiation.

The variation of the wavelength of composition modulation with ageing time at isothermal ageing temperatures of 773, 823, 873 and 923 K for alloys A, B and C are shown in Figs 13 to 15. All the three alloys exhibited similar behaviour. Initially the wavelength remained constant, then after some ageing time it started to increase. The initial constant wavelength λ_m, was found to increase with increasing ageing temperature. Also, as the ageing temperature was increased, coarsening was found to commence earlier. The fact that at 923 K there is no clearly identifiable λ_m can be attributed to the fact that at this temperature the coarsening set in very early.

These results are in accord with Cahn's [13] theory of spinodal decomposition according to which there is a composition wave, with a wavenumber β_m, which has the maximum amplification factor and hence will be in a dominant position to grow as compared to the other waves. The magnitude of β_m does not change during short ageing periods. A number of other investigators have also reported such constant wavelengths [14–16].

The following equation relates this constant wavelength or wavenumber β_m with the ageing temperature T [17]

$$\beta_m^2 = (T - T_s^*)\, S''/4K \qquad (2)$$

where T_s^* is the coherent spinodal temperature, $S'' = \partial^2 S/\partial C^2$ and K the gradient energy coefficient.

According to this equation, as the ageing temperature is decreased β_m increases, i.e. λ_m decreases. This is corroborated by the results of the present investigation except for alloy D which showed an anomalous behaviour in that the same value of λ_m was observed at all the ageing temperatures. Carpenter [18] while investigating a series of gold–platinum alloys found that the initial constant wavelength did not change with ageing temperature, whereas Miyazaki *et al.* [16] found the magnitude of the initial constant wavelength to increase with increasing ageing temperature in Fe–Mo alloys.

In a series of alloys spanning the miscibility gap the coherent spinodal temperature of the alloys rise as the composition is shifted from the edges to the centre, reaching the peak for the symmetric alloy. At any given ageing temperature T, the magnitude of

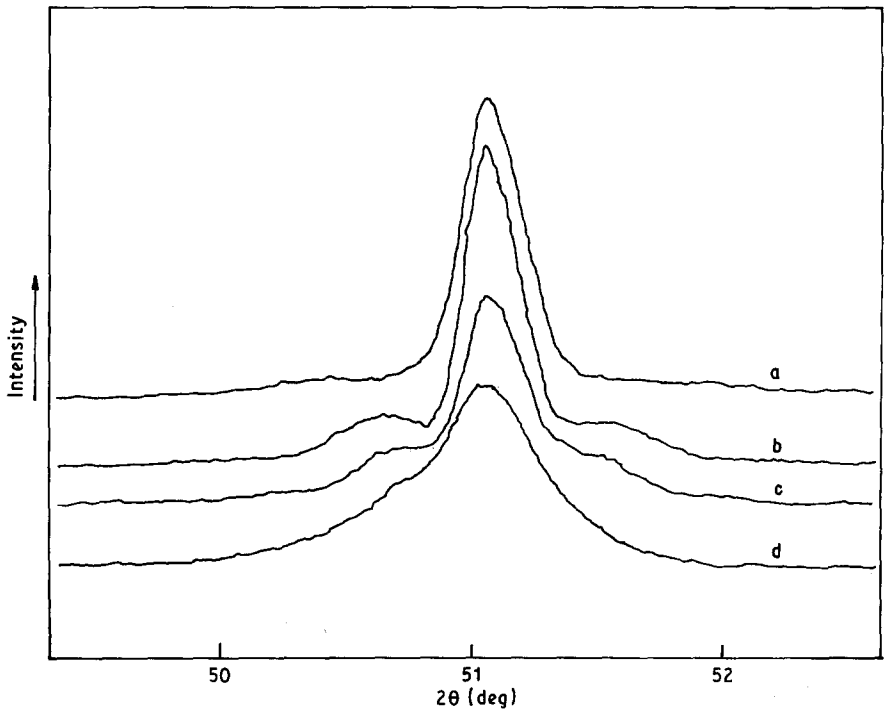

Figure 11 X-ray diffraction profiles of alloy B aged for various durations at 873 K. (a 1.8 k sec, b 14.4 k sec, c 54 k sec, d 180 k sec).

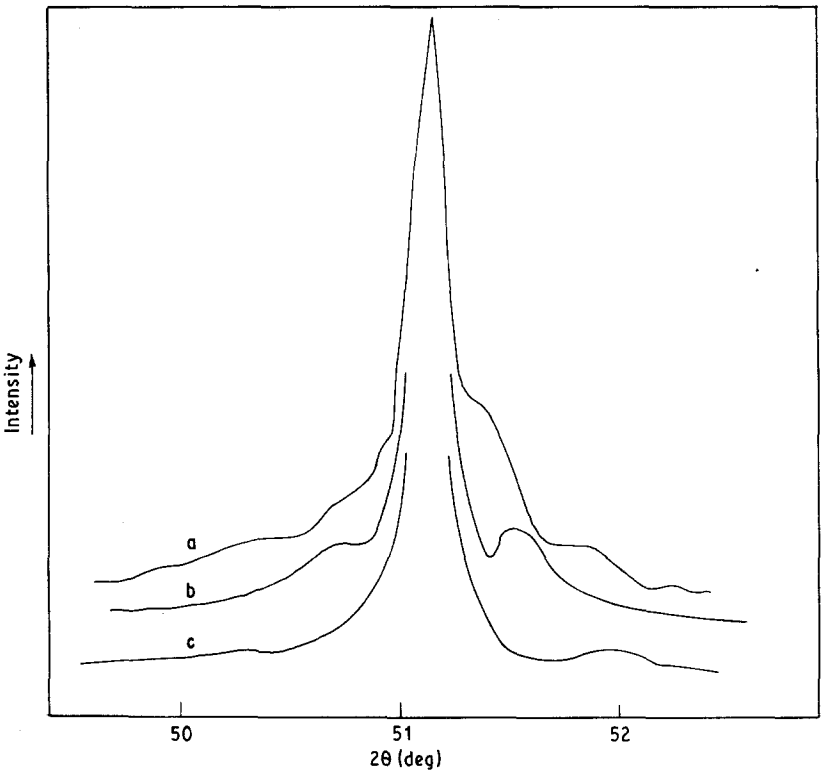

Figure 12 α_1 components of XRD profiles after Rachinger analysis for alloy C aged for various durations at 873 K. (a 108 k sec, b 36 k sec, c 600 sec).

$(T - T_s^*)$ will be a maximum for the symmetric alloy, therefore as from Equation 2 β_m will also be a maximum for the symmetric composition and decrease as the composition moves away on either side. This is reflected in the λ_m values for the three alloys investigated here. At the ageing temperature of 773 K, the λ_m values for the three alloys A, B and C are 5.8, 4.6 and 5.4 nm, respectively. λ_m is least for the symmetric alloy B and higher for the asymmetric alloys on either side, namely A and C.

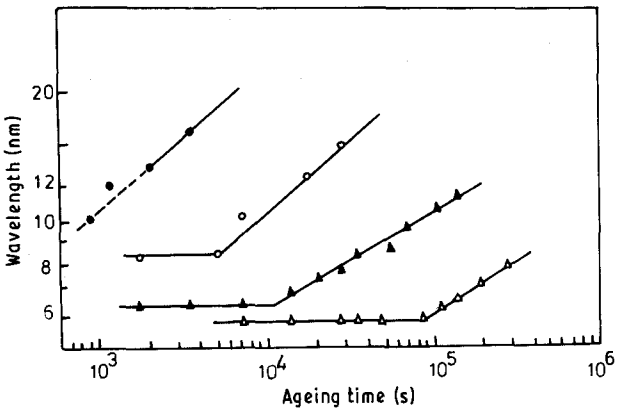

Figure 13 Variation of wavelength of composition modulation with ageing time at various ageing temperatures for alloy A [8]. (● 923 K, ○ 873 K, ▲ 823 K, △ 773 K).

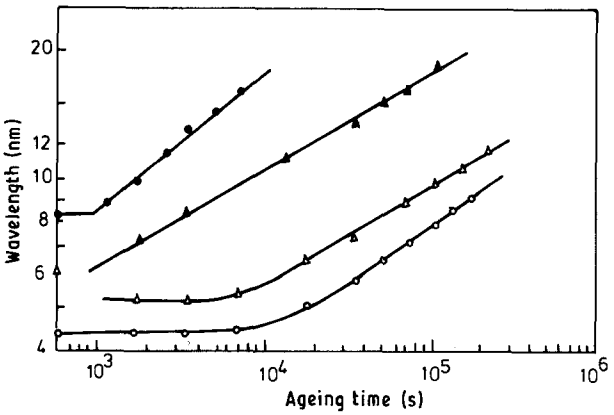

Figure 14 Variation of wavelength of composition modulation with ageing time at various ageing temperatures for alloy B. (● 923 K, ▲ 873 K, △ 823 K, ○ 773 K).

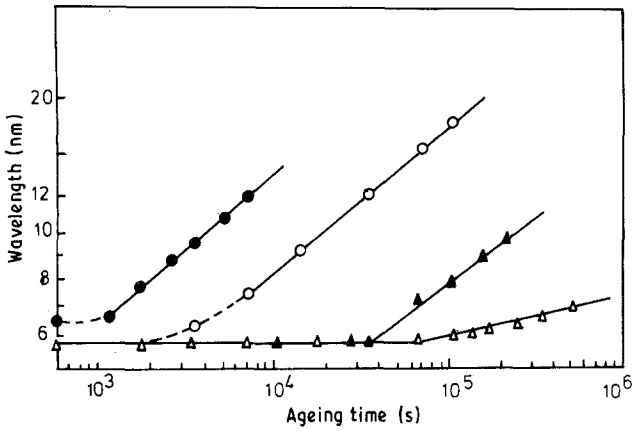

Figure 15 Variation of wavelength of composition modulation with ageing time at various ageing temperatures for alloy C. (● 923 K, ○ 873 K, ▲ 823 K, △ 773 K).

At a given ageing temperature, coarsening starts earlier for alloy B than for alloys A or C. In alloys A and C the wavelength remained constant for more than 72 k sec at the ageing temperature of 773 K and the coarsening started thereafter. In alloy B, however, at the same ageing temperature, the coarsening started after about 7.2 k sec. This can be attributed to the difference in the thermodynamic driving force between the symmetric and asymmetric alloys as explained below.

The transformation in spinodal decomposition is essentially a diffusional process. The rate of decomposition is proportional to the interdiffusion flux J, which is given by the following equation [17], if we

neglect the terms strain energy and gradient energy coefficients

$$J = Mf'' \quad (3)$$

The term f'', the second derivative of free energy with composition, has the highest magnitude for the symmetric alloy as compared to any asymmetric alloy. At a given temperature, therefore, the symmetric alloy will have a higher interdiffusional flux when compared with any asymmetric alloy leading to faster transformation in the symmetric alloy.

The values of f'' were estimated for the three alloys from the relation [17]

$$\beta_m^2 = -(f'' + 2\eta^2 Y)/2K \quad (4)$$

where η is the linear expansion per unit composition change and Y the elastic constant. The gradient energy coefficient K was theoretically estimated from the following relation [19, 20]

$$K = \omega\Psi^2/2 \quad (5)$$

where

$$\omega = 4h_{0.5}^{M} \quad (6)$$

and

$$\Psi = 3^{-1/2} r_0 \quad (7)$$

Here $h_{0.5}^{M}$ is the integral heat of mixing per unit volume at $C = 0.5$, Ψ the r.m.s. interaction distance and r_0 the interatomic distance. By taking the value for heat of mixing for copper nickel alloys from Hultgren [21], the gradient energy coefficient was estimated to be 1.062×10^{-10} J m^{-1} for an interatomic distance of 0.356 nm, taken as the average value for the alloys investigated here.

By taking the value of $\eta = 2.6 \times 10^{-2}$ [10] and $\gamma = 11.48 \times 10^{10}$ N m^{-2} [22], f'' was estimated as -6.961×10^8, -9.731×10^8 and -7.691×10^8 J m^{-3} for alloys A, B and C, respectively, for values taken from Figs 13 to 15 for ageing temperature 773 K. The magnitudes of f'' compare favourably with those estimated for Ni–Cu–Si [20]. It can be seen that the magnitude of f'' is more for alloy B than for alloys A or C.

3.2.3. Coarsening kinetics

The rate of increase of the wavelength in the coarsening regime for a given alloy increased with the isothermal ageing temperature. The data used in Figs 13 to 15 have been replotted in Figs 16 to 18 to fit into the following equation

$$\lambda^3 - \lambda_m^3 = k(t - t_0) \quad (8)$$

where λ is the wavelength of composition modulation at time t, t_0 is the time at which coarsening starts and λ_m is the initial constant wavelength. Linear plots at all the isothermal ageing temperatures indicate that Lifshitz–Slyozov [23] and Wagener [24] coarsening rule is obeyed. Therefore coarsening can be assumed to proceed by a volume diffusion controlled mechanism.

The rate constants, k, determined from the slopes of the linear plots in Figs 16 to 18 for the three alloys at

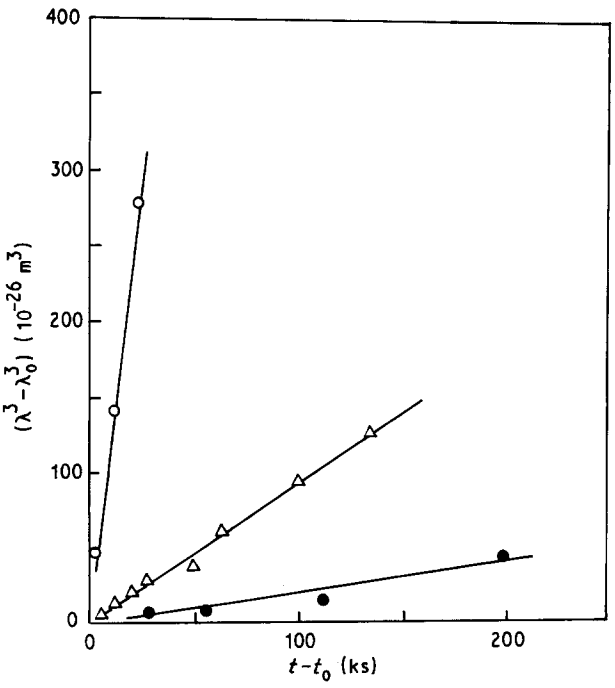

Figure 16 Plot of $(\lambda^3 - \lambda_m^3)$ against $(t - t_0)$ at various ageing temperatures for alloy A [8]. (○ 873 K, △ 823 K, ● 773 K).

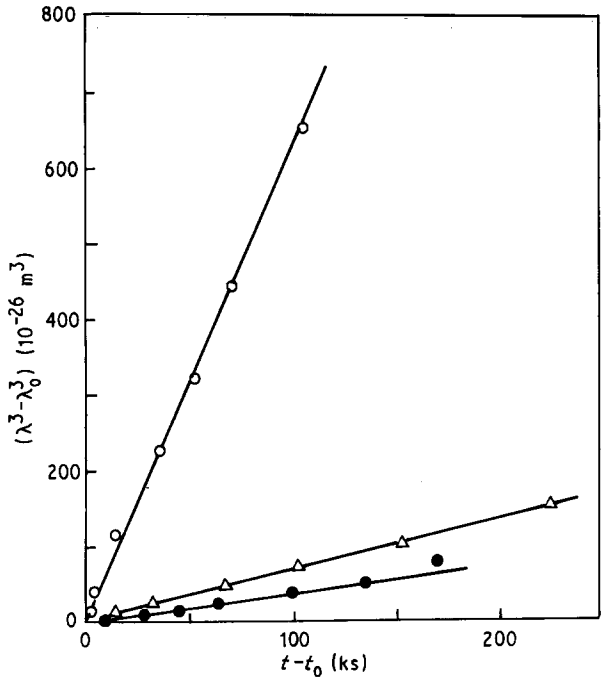

Figure 17 Plot of $(\lambda^3 - \lambda_m^3)$ against $(t - t_0)$ at various ageing temperatures for alloy B. (○ 873 K, △ 823 K, ● 773 K).

the ageing temperatures of 773, 823 and 873 K, as also for 923 K which is not shown in the above figures are plotted in Fig. 19 as k^3 against $1/T$. These are, again, straight lines for all the three alloys. All three curves have more or less the same slope. The activation energy as determined from these slopes is 277.82 kJ mol^{-1}. Activation energy for diffusion in Cu–Ni system is found to be of the same order as estimated here.

Spinodal decomposition in alloys similar to B in the present investigation have been studied by Bower *et al.* [5] and also by Saunderson *et al.* [7]. The former

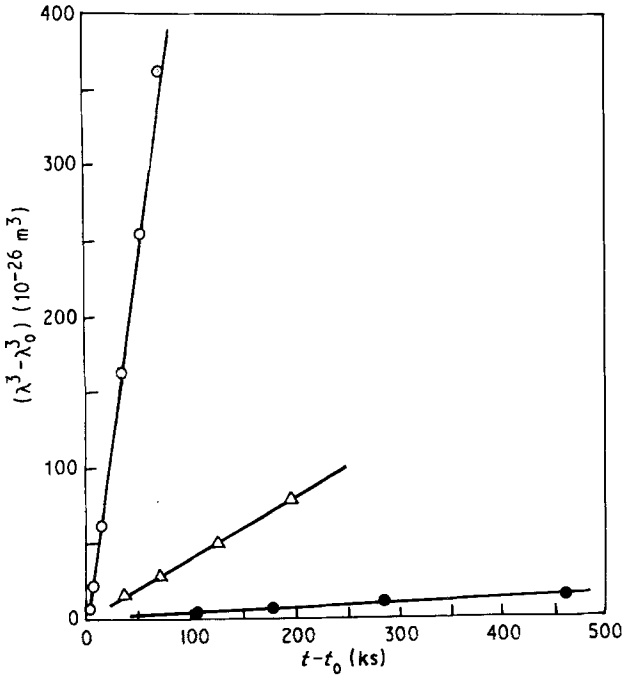

Figure 18 Plot of $(\lambda^3 - \lambda_m^3)$ against $(t - t_0)$ at various ageing temperatures for alloy C. (○ 873 K, △ 823 K, ● 773 K).

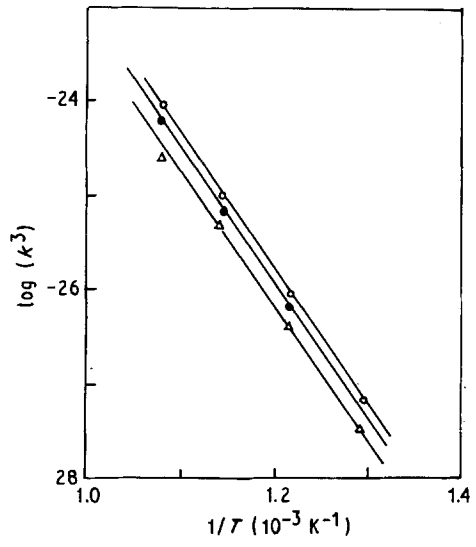

Figure 19 Plot of log (k^3) against $1/T$ for alloys A (○), B (●) and C (△).

have reported the results of their study at 823 K which is similar to the one obtained in the present investigation. There is an initial period during which the wavelength remains constant. This is followed by a coarsening regime during which $\lambda \alpha\ t^{1/3}$ law is obeyed.

Saunderson *et al.* [7] have investigated the variation in wavelength with ageing time at three temperatures of 823, 873 and 923 K. Their results at 823 and 923 K are similar to the ones observed in the present investigation. AT 873 K, they have, however, observed three stages of coarsening which has not been observed in the present investigation. This may be because of the much shorter ageing times employed in the present investigation as compared to that of Saunderson *et al.* [7].

3.2.4. Asymmetry of the side bands

The side bands of all the three alloys investigated were found to be asymmetric with regard to their intensity. While the X-ray diffraction profiles of alloy A showed the side bands on the low angle side to be of higher intensity, those of alloy C showed higher intensity for side bands on the high angle side. In the diffraction profiles of alloy B the side bands on the low angle side were marginally more intense than those on the high angle side. This is represented in Fig. 20. The Bragg peaks are omitted for clarity.

Other workers too have observed asymmetric side bands in the diffraction profiles of alloys with modulated structures. While the theory of Daniel and Lipson [11, 25] is able to predict correctly the average wavelength of composition modulation, it fails on two other considerations. Firstly, the theory predicts side bands which are as sharp as the Bragg peak itself, whereas in practice the side bands are diffuse in nature. Secondly, it predicts symmetric side bands whereas in practice the side bands are never mirror images of each other. These drawbacks arise due to the assumption of a sinusoidal variation in lattice parameter. Hargreaves [26] modified the Daniel–Lipson formula to include square wave modulations. He assumed a crystal in which layers with one parameter (say *C*) elongated are followed by an equal number of layers with this parameter contracted, the other two (*a* and *b*) being the same as in the homogeneous alloy. These distortions alternated with the undistorted part of the crystal. This theory also fails to predict either the asymmetry or the diffuse nature of the side bands. Failure is again due to the assumption of perfect periodicity and symmetric distortion just as in the case of Daniel–Lipson theory. Tiedema, Bowman and Burgers [27] therefore considered the case of asymmetrical distortion. They considered a mosaic lattice in which distortion along, say, *a* axis was considered to consist of *p* unit cells with lattice parameter a_1 along the axis alternating with *q* unit cells with lattice parameter a_2. They showed that when *p* and *q* were unequal the side band intensities were also unequal and when *p* and *q* were equal, the side band intensities were also equal. They assumed that *p* and *q* represented the two phases in equilibrium. Thus, one can estimate the ratio of side band intensities by taking the volume fractions of the phases from the phase diagram. For two alloys when $p:q$ is inverse, the ratio of intensities should also be inverse.

The observations made in the present investigation on the nature of the side bands can be explained on similar lines as above. If we assume *p* and *q* to correspond to the proportions of the γ_1 and γ_2 phases, respectively, we find that the low angle side band should have higher intensity for alloy A. Since *q* is higher for alloy C, then its higher angle side band should be more intense than the low angle side band. In alloy B, *p* and *q* are nearly equal. Therefore, the side bands have almost the same intensities.

The ratio of the intensity of the low angle side band to the high angle side band are given in Table III for the alloys A, B and C. It can be seen from these values that as the ageing time increases the ratio increases for

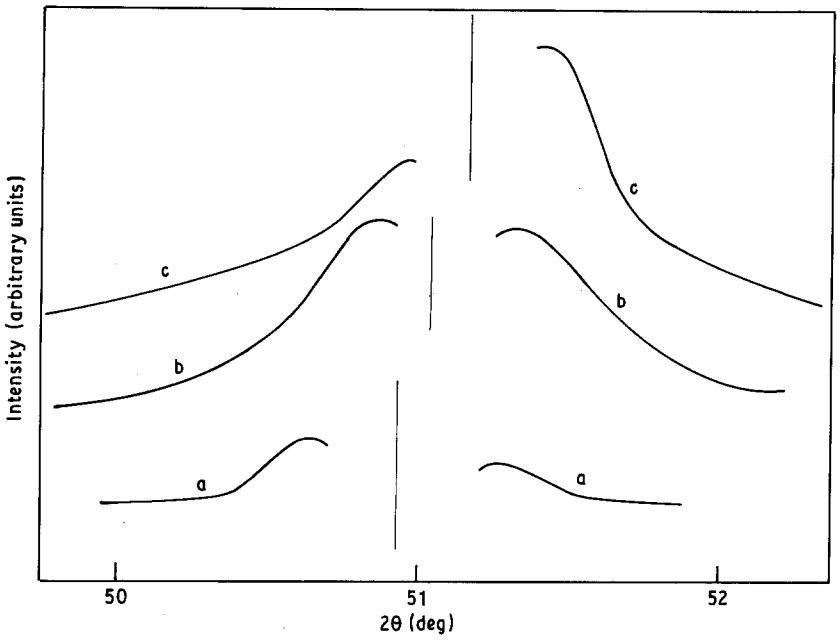

Figure 20 Asymmetry of side bands on XRD profiles (a) alloy A aged for 9 k sec at 973 K, (b) alloy B aged for 36 k sec at 873 K, (c) alloy C aged for 72 k sec at 873 K.

TABLE III Ratio of side band intensities after ageing at 873 K

Alloy	Ageing time (k sec)	Ratio I_L/I_H
A	1.8	1.18
	5.4	1.28
	18	1.31
	28.8	1.59
B	0.6	1.00
	1.8	1.05
	14.4	1.12
	54	1.12
C	0.6	0.94
	36	0.88
	72	0.79
	108	0.75

A and decreases for C. In other words, as the wavelength increases, difference in intensity between the two side bands also increases.

3.3. Transmission electron microscopy

The primary aim of the transmission electron microscopic investigation was to compare the microstructural features of the symmetric and asymmetric alloys. As reported elsewhere [8], the alloy A showed typical features of spinoidal alloys such as periodic array of phases and absence of preferential precipitation at microstructural inhomogeneities such as grain boundaries and dislocations. No connectivity was, however, observed between the γ_2 precipitates. This was attributed to the low volume fraction (less than 10%) of γ_2 phase.

Alloy B on the other hand showed good interconnectivity amongst particles of the γ_1 phase as well as those of γ_2 phase. This is indicated in Fig. 21 which shows the microstructures at different ageing times at the ageing temperatures of 873 K. The bright and dark phases, namely γ_1 and γ_2 are in almost equal proportions.

The microstructure of alloy C was very similar to that of alloy B in that the precipitating phases exhibited a high degree of interconnectivity. This is indicated in Fig. 22a, b, and c for the samples aged for 7.3, 36 and 72 k sec respectively at 823 K. The darker phase (γ_2) is, however, now in a higher proportion than the brighter phase.

The interconnectivity amongst the precipitate particles of the bright region, i.e., γ_1, appears to decrease with progressive ageing. It can be seen that while in Fig. 22a the γ_1 particles are well connected, in Fig. 22c they are elongated in one direction and more or less isolated from each other. Coarsening appears to be taking place by a process of joining up of the ligands. This can be seen in Fig. 23 where the darker γ_2 bands appear to be joining up. In some places one can see projections developing on the edge of the ligand. Presumably they grow towards and join up with the neighbouring ligand. This may be the cause of the loss of interconnectivity amongst the γ_1 phase particles. Saunderson *et al.* [7] from their study of a series of Cu–Ni–Cr alloys concluded that the γ_1 phase was always the one with interconnectivity which was maintained till very late stages of coarsening. The present investigation suggests, however, that during coarsening the major phase increases its connectivity and isolates the minor phase.

Coarsening in alloy A was found [8] to proceed by a process of clustering and coalescence of discrete particles. This was explained in a qualitative manner using Kachathuryan's [28] analysis. The exact mechanism of coarsening in alloys B and C is not very clear. These, after very short periods of ageing, produced well connected distribution of particles. As the ageing progressed these coarsened but connectivity remained. At all temperatures, a distribution of particle sizes existed. Larger particles grew by the dissolution of smaller particles in selected area, thereby joining adjacent particles. The presence of a large number of discontinuities in the periodicity appears to promote the growth process. Similar discontinuities have been reported by Butler and Thomas [29] in Cu–Ni–Fe

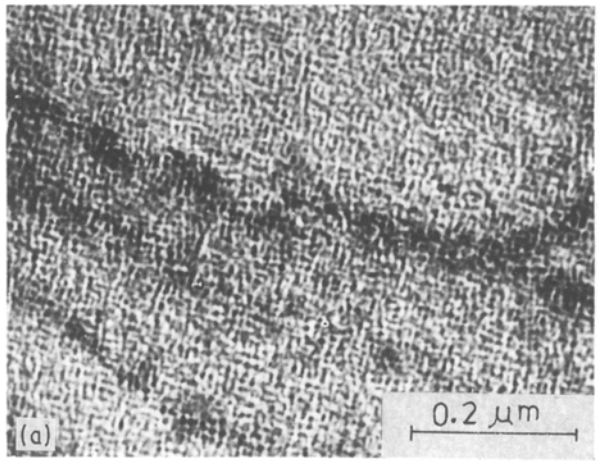

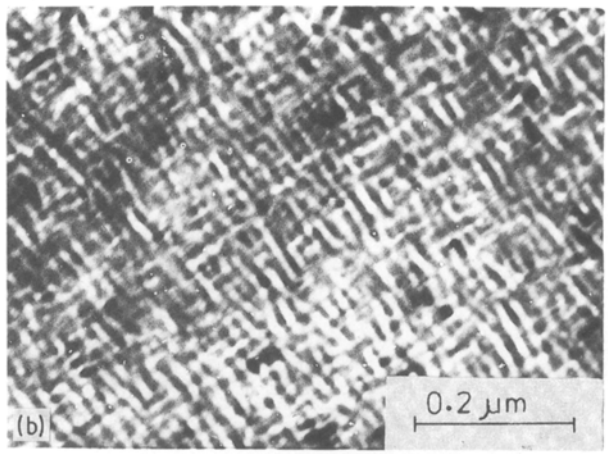

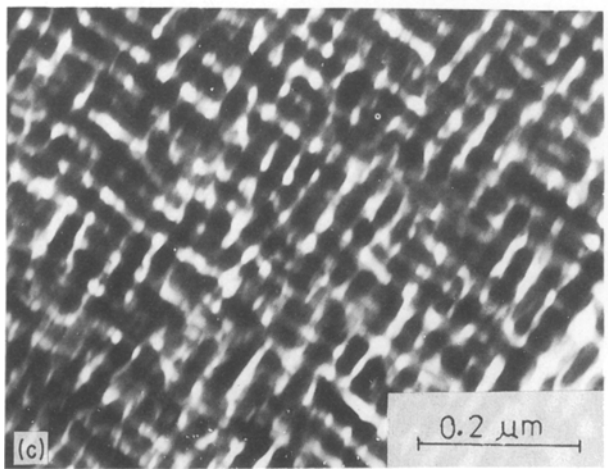

Figure 21 Microstructures of alloy B after ageing at 873 K for (a) 600 sec (b) 7.2 k sec and (c) 72 k sec.

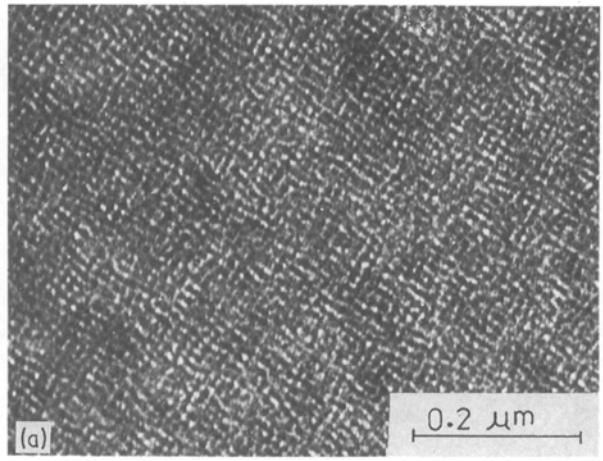

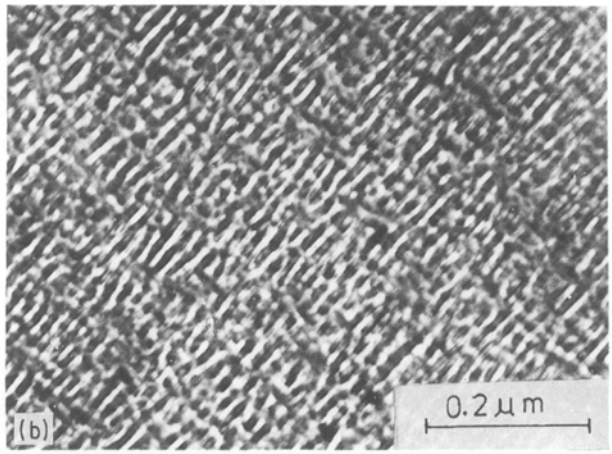

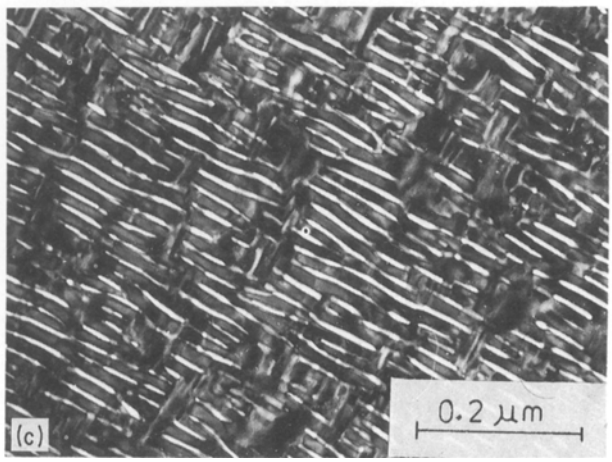

Figure 22 Microstructures of alloy C after ageing at 873 K for (a) 8.2 k sec, (b) 36 k sec, and (c) 72 k sec.

alloys and by de Vos [30] in Al–Ni–Co alloys. The latter reported that these discontinuities gave a visual impression of dislocations. He noted that the wavelength increased when these dislocations climbed.

A comparison of the microstructures of the three alloys reveals that in A the dark constituent is the minor phase whereas in C the brighter constituent is the minor phase. In B both the dark and bright constituents appear to be in equal proportions. The X-ray diffraction studies have revealed that (Table III) A has γ_2 as the minor phase and C has γ_1 as the minor phase. This suggests that the brighter region is the copper-rich γ_1 phase and darker region is the nickel-rich γ_2 phase. The brightness (in bright field) of the copper-rich phase may be due to preferential thinning during electropolishing.

4. Conclusions

The conclusions are as follows.

(1) X-ray diffraction and transmission electron microscopic results show that alloys A and C are of asymmetric composition while B is of symmetric composition.

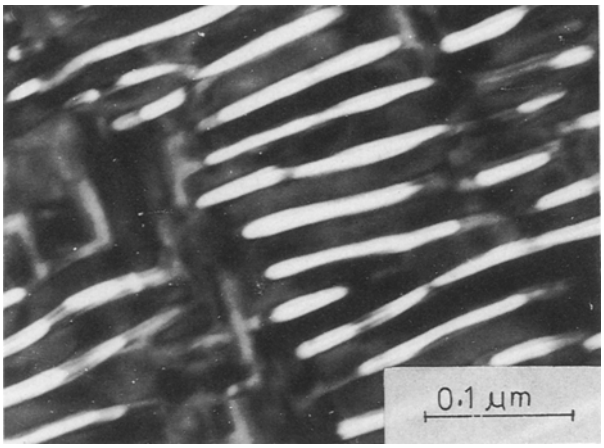

Figure 23 Microstructure of alloy C aged for 72 k sec, at 873 K.

(2) Kinetics of spinodal decomposition is found to be faster for the symmetric alloy than for the asymmetric ones. This could be explained in terms of the interdiffusion flux.

(3) The initial constant wavelength was smaller for the symmetric alloy than for the asymmetric ones in accord with Cahn's model.

(4) The asymmetry of side bands in the X-ray diffraction profiles can be related to the proportion of phases in the alloy on undergoing spinodal decomposition.

(5) Alloys B and C show a high degree of interconnectivity amongst the phases γ_1 and γ_2, however, during coarsening the major phase isolates the minor phase.

Acknowledgements

The work was carried out during the stay of one of the authors (PPR) in the Department of Metallurgical Engineering, IIT Bombay under Quality Improvement Programme of the Government of India. He, therefore, wishes to express his sincere thanks to the Principal, Karnataka Regional Engineering College, Surathkal, for granting him leave which made this work possible.

References

1. J. L. MEIJERING, G. W. RATHENAU, M. G. VAN DER STEEG and P. B. BRAUN, *J. Inst. Met.* **84** (1950–56) 118.
2. J. MANENC, *Acta Metall.* **6** (1958) 145.
3. C. K. WU and G. THOMAS, *Met. Trans.* **8A** (1977) 1911.
4. A. CHOU, A. DUTTA, G. H. MEIER and W. A. SOFFA, *J. Mater. Sci.* **13** (1978) 541.
5. D. BOWER, G. W. LORIMER, I. SAUNDERSON and P. WILKES, *Met. Tech.* **7** (1980) 120.
6. R. KNIGHTS and P. WILKES, *Met. Trans.* **4** (1973) 2389.
7. R. I. SAUNDERSON, P. WILKES and G. W. LORIMER, *Acta Metall.* **26** (1978) 1357.
8. P. PRASAD RAO, B. K. AGRAWAL and A. M. RAO, *J. Mater. Sci.* **21** (1986) 3759.
9. W. A. RACHINGER, *J. Sci. Instrum.* **25** (1948) 254.
10. W. B. PEARSON, "Handbook of lattice spacings and structures of metals" (Pergamon, New York, 1958) p. 592.
11. V. DANIEL and H. LIPSON, *Proc. R. Soc.* **A181** (1943) 368.
12. M. HILLERT, *Acta Metall.* **9** (1961) 525.
13. J. W. CAHN, *Trans. Met. Soc. AIME* **242** (1968) 166.
14. R. J. LIVAK and G. THOMAS, *Acta Metall.* **19** (1971) 497.
15. D. E. LAUGHLIN and J. W. CAHN, *ibid.* **23** (1975) 329.
16. T. MIYAZAKI, S. TAKAGISHI, H. MORI and T. KOZAKAI, *ibid.* **28** (1980) 1143.
17. J. E. HILLIARD, Spinodal Decomposition, in "Phase Transformations", edited by H. I. Aaronson (American Society for Metals, Metals Park, OH, 1970) pp. 497–560.
18. R. W. CARPENTER, *Acta Metall.* **15** (1967) 1567.
19. H. E. COOK and J. E. HILLIARD, *J. Appl. Phys.* **40** (1969) 2191.
20. T. MIYAZAKI, T. SHINOZAWA, H. MURAYAMA and H. MORI, *Trans. Jpn. Inst. Met.* **17** (1976) 181.
21. R. HULTGREN, P. D. DESAI, D. T. HAWKINS, M. GLEISER and K. K. KELLY, "Selected values of the thermodynamic properties of binary alloys" (American Society for Metals, Metals Park, OH, 1973) p. 763.
22. C. J. SMITHELS, "Metals Reference Book" (Butterworths, London, 1976).
23. I. M. LIFSHITZ and V. V. SLYOZOV, *J. Phys. Chem. Solids* **19** (1961) 35.
24. C. WAGNER, *Z. Elektrochem.* **65** (1961) 581.
25. V. DANIEL and H. LIPSON, *Proc. R. Soc.* **182** (1944) 378.
26. M. E. HARGREAVES, *Acta Crystallogr.* **4** (1951) 301.
27. T. J. TIEDEMA, J. BOUMAN and W. G. BURGERS, *Acta Metall.* **5** (1957) 310.
28. A. G. KATCHATURYAN, *Phys. Status. Solidi* **35** (1969) 19.
29. E. P. BUTLER and G. THOMAS, *Acta Metall.* **18** (1970) 347.
30. G. de VOS, *J. Appl. Phys.* **37** (1966) 1100.

Received 4 January
and accepted 23 August 1989